Materials Research Bulletin 46 (2011) 278–284

Contents lists available at ScienceDirect

Materials Research Bulletin

journal homepage: www.elsevier.com/locate/matresbu

The control of the diameter and length of α-MnO_2 nanorods by regulation of reaction parameters and their thermogravimetric properties

Polona Umek [a,*], Romana Cerc Korošec [b], Alexandre Gloter [c], Urša Pirnat [d]

[a] Jožef Stefan Institute, Jamova cesta 39, 1000 Ljubljana, Slovenia
[b] Faculty of Chemistry and Chemical Technology, University of Ljubljana, Aškerčeva 5, 1000 Ljubljana, Slovenia
[c] Laboratoire de Physique des Solides, Université Paris Sud, CNRS UMR8502, Orsay, France
[d] University of Nova Gorica, Vipavska 13, PO Box 301, Rožna Dolina, 5000 Nova Gorica, Slovenia

ARTICLE INFO

Article history:
Received 17 May 2010
Received in revised form 21 September 2010
Accepted 22 October 2010
Available online 30 October 2010

Keywords:
A. Oxides
B. Chemical synthesis
C. Electron microscopy
C. Thermogravimetric analysis (TGA)

ABSTRACT

α-MnO_2-type single-crystal nanorods were synthesized under hydrothermal conditions based on the redox reaction of $KMnO_4$ in an acidic environment. Several reaction parameters, like the reaction temperature, the reaction time and the concentration of $KMnO_4$ in the reaction mixture, were varied in order to determine their impact on the structure, the dimensions of the synthesized nanorods, and as well on their thermogravimetric properties. It was found that the reaction time has no significant influence on the diameter, although it has a strong influence on the length of the obtained nanorods. On the other hand, the concentration of $KMnO_4$ in the reaction mixture has a strong impact on both the diameter and the length. With an increasing concentration of $KMnO_4$ in the reaction mixture the average lengths and diameters of the isolated MnO_2 nanorods are reduced. The change in dimensions of the synthesized nanorods is reflected in their thermogravimetric properties.

1. Introduction

The cognition that the size of nanoparticles determines physical properties of materials [1–3] has pushed synthetic chemists to focus on the controlled synthesis (in terms of size) of various nanostructured materials with the aim to control the size of nanoparticles by regulation of reaction parameters [4]. One of the materials of interest is MnO_2 mainly due to combined chemical and physical properties [5] that are exploited in a wide range of technological applications, such as the cathode material in alkaline and rechargeable batteries, molecular sieves, catalysts and sensors [6–9].

MnO_2 can be synthesized by redox reactions of MnO_4^- and/or Mn^{2+} in solution via several different synthesis methods, i.e., hydrothermal [10–12], reflux [13], electrochemical [14] and sonochemical [15]. With the careful selection of the reactants and with pH regulation one can influence not only the formation of a desired polymorphic form but also the morphology and the chemical composition.

The simplest approach to the synthesis of MnO_2 nanostructures is the hydrothermal decomposition of $KMnO_4$ in an acidic environment which typically yields α-MnO_2 nanorods, regardless of the acid [12,16] used for the preparation of the reaction mixture. By introducing slight changes to the reaction mixture, for instance, with the addition of Fe^{3+} ions or the presence of a Si substrate, MnO_2 nanotubes can be obtained as well [17,18]. Although a lot of effort has been put into the control of the morphology and the polymorph type, there are not a lot of studies focusing on the diameter and length control of α-MnO_2 nanostructures. As already mentioned, the length and the diameter of nanoparticles have a strong influence on physical properties of materials [1–3] and for this reason the control of the diameter and the length at resulting nanoparticles is very important.

In this work, we demonstrate for the first time that by careful regulation of reaction parameters at hydrothermal decomposition of $KMnO_4$ in acidic media, the diameter and length of synthesized α-MnO_2 nanorods can be controlled. The major impact on the length and diameter of α-MnO_2 nanorods comes from the $KMnO_4$ concentration in the reaction mixture, while the reaction temperature has a significant impact on the secondary structure. The differences in the morphology of the synthesized products (i.e., nanorods and nanoparticles) are reflected in the course of their thermal decomposition.

2. Experimental

2.1. Synthesis

For a single reaction series only one reaction parameter was altered, while all the others were kept constant:

---

* Corresponding author.
E-mail address: polona.umek@ijs.si (P. Umek).

0025-5408/$ – see front matter © 2010 Elsevier Ltd. All rights reserved.
doi:10.1016/j.materresbull.2010.10.012

2.2. Reaction temperature

Reactions were performed in the temperature range between 70 and 170 °C (in steps of 20 °C). During a typical synthesis, $KMnO_4$ (1.6 mmol) was first dissolved in distilled water (18 mL) with the help of an ultra-sonic bath, after which concentrated H_2SO_4 (0.8 mL) was added. The reaction mixture was stirred for another 5 min and then transferred into a Teflon-lined autoclave and maintained at a constant temperature for 17 h. When cooled to room temperature, an isolated precipitate was obtained by centrifugation; this was then washed with distilled water (20 mL) and dried over night at 100 °C. The isolated products were labelled as **T-70**, **T-90**, **T-110**, **T-130**, **T-150** and **T-170**, where the numbers stand for the reaction temperature at which the reactions were performed.

2.3. $n(KMnO_4)$ and $V(H_2SO_4)$

In this reaction batch the reactions were preformed with different starting concentrations of $KMnO_4$, i.e., 1.6, 4, 6 and 8 mmol. The reactions were performed at 150 °C for 17 h. In this case for $n \geq 4$ mmol, the volume of added sulfuric acid was also altered. In order to dissolve the $KMnO_4$, 10 mL of distilled water was added to the required amount of $KMnO_4$ and then 2 mL of H_2SO_4 for $n = 4$ mmol (3 mL for $n = 6$ mmol and 4 mL for $n = 8$ mmol) were added. Finally, the reaction mixtures were diluted with distilled water up to 18 mL. The products were labelled **n-1.6**, **n-4**, **n-6**, and **n-8**, where the numbers stand for $n(KMnO_4)$.

2.4. Reaction time

The reaction mixtures were kept at 150 °C for 6, 17 and 24 h. The products were labelled **t-6**, **t-17**, and **t-24**, where the numbers relate to the reaction times.

The reader should note that the labels of the products **t-17**, **n-1.6** and **T-150** refer to the same product that was synthesized at 150 °C from 1.6 mmol of $KMnO_4$ for 17 h. In addition, all the reactions were preformed in 23-mL, Teflon-lined, stainless-steel autoclaves that were filled up to 84% of their volume.

2.5. Characterization

Field-emission scanning electron (FE-SEM; Carl Zeiss, Supra 35LV) and transmission electron microscopes (TEM; Jeol 2010 and Jeol 2100, 200 keV) were used for the morphology characterization and the nanorods' lengths and diameters measurements. The elemental compositions of the samples were investigated with a FE-SEM equipped with an EDX (energy-dispersive X-ray spectrometer) element analysis system. The specimens for the TEM investigations were prepared by dispersing the sample in MeOH with the help of an ultrasonic bath and depositing a droplet of the dispersion on a lacey-carbon-coated copper grid. For the diameter (TEM) and length (SEM) measurements a total of 60–100 nanorods were checked. The powder X-ray diffraction (XRD) patterns were obtained on a Bruker AXS D4 Endeavor diffractometer using Cu K_α radiation (1.5406 Å) in the 2θ range from 10 to 70°. Thermogravimetric (TG) measurements were performed on a Mettler Toledo Instrument TGA/SDTA 851^e from room temperature up to 1100 °C with a heating rate of 5 K min^{-1}. The samples with initial weights of around 5 mg were placed in 70-μL alumina crucibles. Argon with a flow rate of 100 mL min^{-1} was used as a purge gas. The baseline was subtracted in all cases. The BET specific surface areas of the samples were measured at −196 °C with a TRISTAR 3000 automated gas-adsorption analyzer.

3. Results and discussion

By careful regulation of reaction parameters beside the morphology and the chemical composition also the size of resulted nanoparticles can be controlled as well [4]. In our experimental studies, that involved hydrothermal decomposition of $KMnO_4(aq)$ in acidic media the reaction temperature ($90\,°C \leq T \leq 170\,°C$), the reaction time ($6\,h \leq t \leq 24\,h$) and the concentration of $KMnO_4$ ($1.6\,mmol \leq n \leq 8\,mmol$) in the reaction mixture were varied in order to modify the average diameters and lengths of α-MnO_2 nanorods.

In general, an aqueous solution of $KMnO_4$ in acidic media yields MnO_2 via two different reaction pathways. As a strong oxidizing agent, $KMnO_4(aq)$ oxidizes water (reaction (1)), and following the first reaction pathway, a permanganate anion is directly reduced to MnO_2 (reaction (2)) [19]. The reaction itself is catalyzed by light, acid and MnO_2 [20].

$$2H_2O \rightarrow O_2(g) + 4H^+(aq) + 4e^- \tag{1}$$

$$MnO_4{}^-(aq) + 4H^+(aq) + 3e^- \rightarrow MnO_2(s) + 2H_2O \tag{2}$$

In solutions with pH < 1, a competitive reaction takes place: the permanganate anion is first reduced to $Mn^{2+}(aq)$ (reaction (3)) and in the next step, a comproportionation reaction between $MnO_4{}^-(aq)$ and $Mn^{2+}(aq)$ (reaction (4)) also yields MnO_2 [19].

$$MnO_4{}^-(aq) + 8H^+(aq) + 5e^- \rightarrow Mn^{2+}(aq) + H_2O \tag{3}$$

$$MnO_4{}^-(aq) + Mn^{2+}(aq) + H_2O \rightarrow 2MnO_2(s) + 4H^+(aq) \tag{4}$$

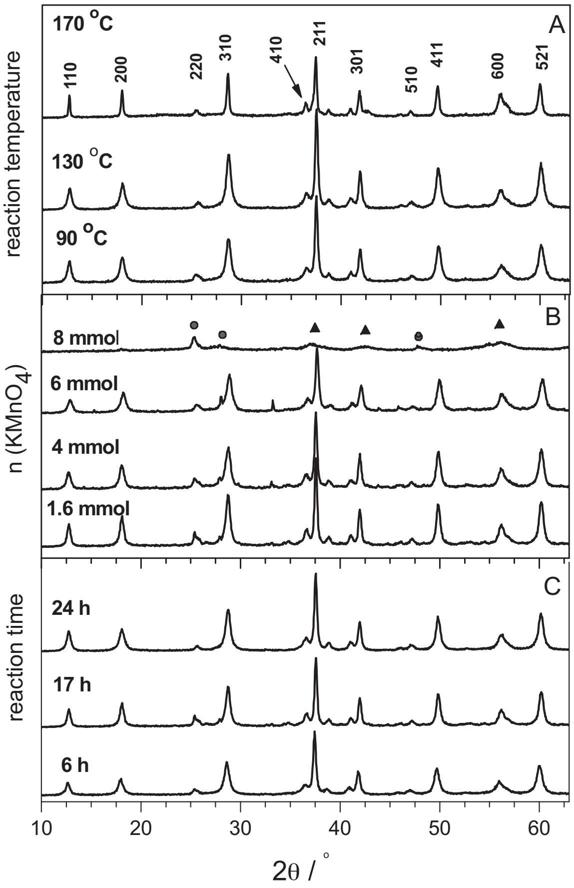

Fig. 1. XRD spectra of MnO_2 nanorods obtained at different: (A) reaction temperatures (90 (**T-90**), 130 (**T-130**) and 170 °C (**T-170**)), (B) starting amounts of $KMnO_4$ ($n(KMnO_4)$: 1.6 (**n-1.6**), 4 (**n-4**), 6 (**n-6**) and 8 mmol (**n-8**)) (● Mn_3O_4, ▲ MnO_2), and (C) reaction times (6 (**t-6**), 17 (**t-17**), and 24 h (**t-24**)), respectively.

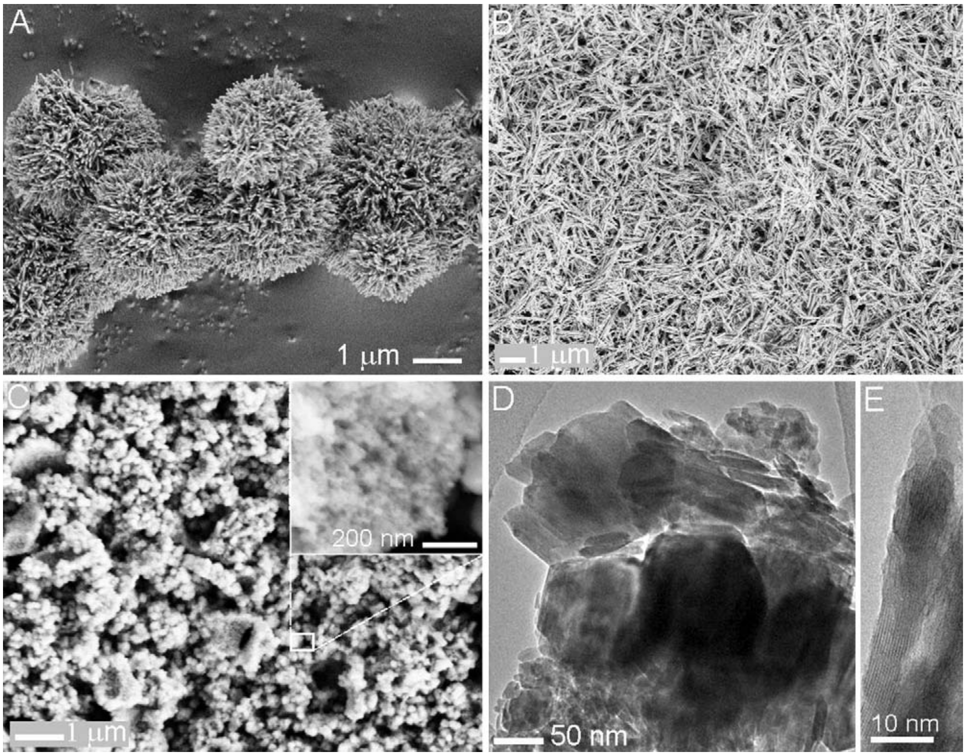

Fig. 2. SEM and TEM images of products synthesized at different reaction temperatures: (A) at 90, (B) at 150, and (C–E) at 170 °C. The inset in the image C is taken at higher magnification of area marked with rectangle in the image C.

The phase purity of the synthesized products was examined by X-ray powder diffraction (Fig. 1). The X-ray patterns from Fig. 1A and C are similar, and all the peaks can be readily indexed to α-MnO_2 (JCPDS, 44-0141). From Fig. 1A, it is unambiguously clear that with the increasing reaction temperature the peaks become narrower, which indicates that the product's crystallinity increases. On the other hand, no significant differences between the XRD patterns of the products synthesized for different reaction times can be observed (Fig. 1C). In contrast, the XRD pattern of the product synthesized from 8 mmol of $KMnO_4$ (**n-8**) differs from the others in this reaction batch (Fig. 1B).

The patterns of **n-1.6**, **n-4** and **n-6** again correspond to the α-MnO_2 structure. However, with increasing $n(KMnO_4)$ in the reaction mixture the peaks become slightly broader, which indicates that the average particle size is reduced. Using the standard Scherrer formula ($d = 0.9\lambda/B\cos\theta$), from the 211 peak we estimated the average nanorod diameters d to be 26 nm (1.6 mol), 24 nm (4 mmol), and 20 nm (6 mmol), which is in good agreement with the measured values (please see Fig. 4). Here, λ = 1.54 Å is the X-ray wavelength, B is the full-width at half-maximum (FWHM) of the Bragg peak, and θ is the Bragg angle. As already mentioned, the XRD pattern of **n-8** ($n(KMnO_4)$ = 8 mmol) is very different compared to the other XRD patterns. The peaks are very broad, which can be related to the small particle size (please see Fig. 3D), and, secondly, the new peaks that appear, correspond to the Mn_3O_4 (ISCD# 031094) crystal structure.

In the next step, we investigated the morphology of synthesized materials using SEM and TEM techniques. From Fig. 2, we can see that the morphology and secondary structure change with the reaction temperature. The products grow in the shape of nanorods (Fig. 2A and B) at reaction temperatures between 90 and 150 °C, while the product synthesized at 170 °C is composed from much smaller particles (Fig. 2C). Only TEM images revealed that the product **T-170** is composed from two types of nanoparticles (regarding the size): (i) smaller nanoparticles of different shapes (Fig. 2D and E) and (ii) bigger nanoparticles with diameters exciding 100 nm (Fig. 2D). In addition, nanorods of the products **T-90** and **T-130** form a secondary structure that resembles that of sea urchins (Fig. 2A). These spherical microstructures range from 2 to 5 μm in diameter.

The influence of the number of mmol of $KMnO_4$ in the reaction mixture (1.6, 4, 6, and 8 mmol) on the morphology was also investigated. From Fig. 3, one can seen that the products **n-1.6**, **n-4** and **n-6** grow in the shape of nanorods, while the morphology of **n-8** (Fig. 3D) differs from the morphology of the other products obtained in this reaction batch. These nanoparticles are crystalline and have a round shape with an average diameter of around 8 nm (see inset in Fig. 3D). This observation agrees well with the very broad peaks in the XRD pattern (Fig. 1B). From comparison of SEM images of **n-1.6**, **n-4** and **n-6** (Fig. 3A–C; images were taken at the same magnification) can be concluded that with an increasing number of mmol of $KMnO_4$ in the reaction mixture, the average length of the obtained nanorods is gradually reduced.

The microscopy investigations using SEM and TEM techniques were not only used for morphology and secondary structure determination, but also for the diameter and length measurements of the synthesized nanoparticles. Typical TEM image of **n-4** is shown in Fig. 4. The diameters of individual nanorods for **n-4** were found to be between 24 and 29 nm what is in a good agreement with the result calculated from Sherrer's formula (24 nm). The inset shown in Fig. 4 is a high resolution image of the nanorod shown in Fig. 4. The interplanar distances of fringes parallel to the rod are 0.69 nm which agrees well with the d value of (1 1 0) planes α-MnO_2 (JCPDS 44-0141). Therefore, the direction of nanorods growth is along the [0 0 1] direction [16,17].

Using both microscopy techniques, the products obtained after different reaction times, at 6 and 24 h (**t-6** and **t-24**), were also investigated. In both cases the products were grown in the nanorod morphology, as shown in Fig. 4B and C. Interestingly, in the sample **t-6** (Fig. 4B), besides nanorods that reach around 2 μm in length,

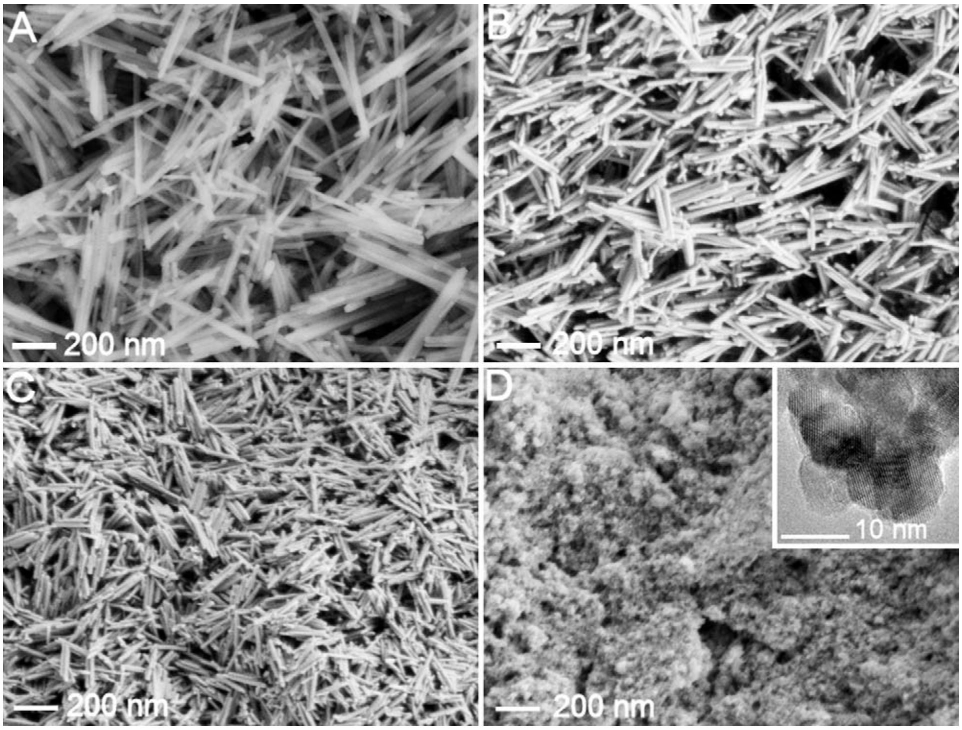

Fig. 3. SEM images of the products synthesized from different amounts of mmol of $KMnO_4$: (A) 1.6 (**n-1.6**), (B) 4 (**n-4**), (C) 6 (**n-6**) and (D) 8 mmol (**n-8**). The inset in figure (D) is a TEM image of a particle that in cross-section measures approximately 6 nm. The products **n-1.6**, **n-4**, **n-6** and **n-8** were synthesized at 150 °C.

also a larger quantity of shorter nanorods (around 100 nm) were observed, when compared to **t-24**. In addition the interplanar distances of the fringes parallel to the rod in Fig. 4C are 0.69 nm.

In Fig. 5, the average diameters and length spans of the nanorods/nanoparticles obtained in this study are shown. The amount of mmol of $KMnO_4$ (Fig. 5C) in the reaction mixture has the highest impact on the nanorods' diameter. The average diameter was reduced by ~45% when the amount of $KMnO_4$ was increased from 1.6 to 6 mmol. Simultaneously, the length of the nanorods also decreased significantly (Fig. 5D). With an increasing amount of $KMnO_4$ in the reaction mixture, not only the average length decreased, but the length span also narrowed. Such significant decrease in the average diameter can be explained by the larger amount of nucleation seeds of smaller diameter that are formed in the reaction solution with a higher number of mmol of $KMnO_4$(aq) in the reaction mixture [4].

From Fig. 5A and E, we can conclude that the reaction temperature and time have no significant impact on the nanorods' diameters. However, nanorods of the desired length can be obtained by careful regulation of the reaction time (Fig. 5F). The fact that with a longer reaction time shorter nanorods are obtained is related to the reactivity of the MnO_2. In an acidic environment the MnO_2 is further reduced to Mn^{2+} (reaction (5)) [20].

$$MnO_2(s) + 4H^+ + 2e^- \rightarrow Mn^{2+}(aq) + 2H_2O \qquad (5)$$

In order to properly evaluate the thermogravimetric results, all the products were submitted for an elemental analysis. The results are summarized in Table 1. In general, all the products contained from 0.12 to 0.15 mol of K^+ per mol of MnO_2, except for **n-8**. This suggests that the product is most probably a mixture of MnO_2 and Mn_3O_4, which was already expected from the XRD pattern. The average sulfur content falls into the range between 0.15 and 4.85 wt.%, where again the sulfur content in **n-8** with 13.4% strongly deviates from the average values. The sulfur detected in the products is part of the hydrogensulfate and/or sulfate anion, originating from the sulfuric acid.

The thermal decomposition of the products, synthesized at different reaction temperatures, occurs in several steps (Fig. 6A). The mass loss in the first step from room temperature to 300 °C is around 3% (Table 2). Within this step there is a gradual mass loss from room temperature to approximately 200 °C, corresponding to the removal of the physically and chemically adsorbed water molecules on the surface.

Dehydration of the trapped water molecules in the tunnels of the hollandite structure take place at higher temperatures, from 200 to 300 °C, due to the high binding energy of the chemisorbed molecules [21]. The thermogravimetric (TG) curve of the product synthesized at 170 °C exhibits another step, from 300 to 430 °C, with a mass loss of approximately 2%. Giovanoli reported that the condensation of OH groups in γ- and ε-MnO_2 leads to the release of much more tightly bound water from 105 to 500 °C, and even

Table 1
Chemical composition of the products prepared under different reaction conditions.

Reaction temperature (°C)	Label	Formula	wt.% S
90	**T-90**	$K_{0.12}MnO_2$	1.25
110	**T-110**	$K_{0.12}MnO_2$	1.12
130	**T-130**	$K_{0.13}MnO_2$	0.76
150	**T-150**[a]	$K_{0.142}MnO_2$	3.53
170	**T-1700**	$K_{0.14}MnO_2$	3.88
n($KMnO_4$) (mmol)			
1.6	**n-1.6**[a]	$K_{0.14}MnO_2$	3.53
4	**n-4**	$K_{0.15}MnO_2$	4.85
6	**n-6**	$K_{0.15}MnO_2$	3.13
8	**n-8**	$K_{0.09}MnO_2$	13.40
Reaction time (h)			
6	**t-6**	$K_{0.13}MnO_2$	1.08
17	**t-17**[a]	$K_{0.15}MnO_2$	3.53
24	**t-24**	$K_{0.12}MnO_2$	0.15

[a] Labels **T-150**, **n-1.6** and **t-17** refer to the same sample that was synthesized at 150 °C for 17 h from 1.6 mmol of $KMnO_4$.

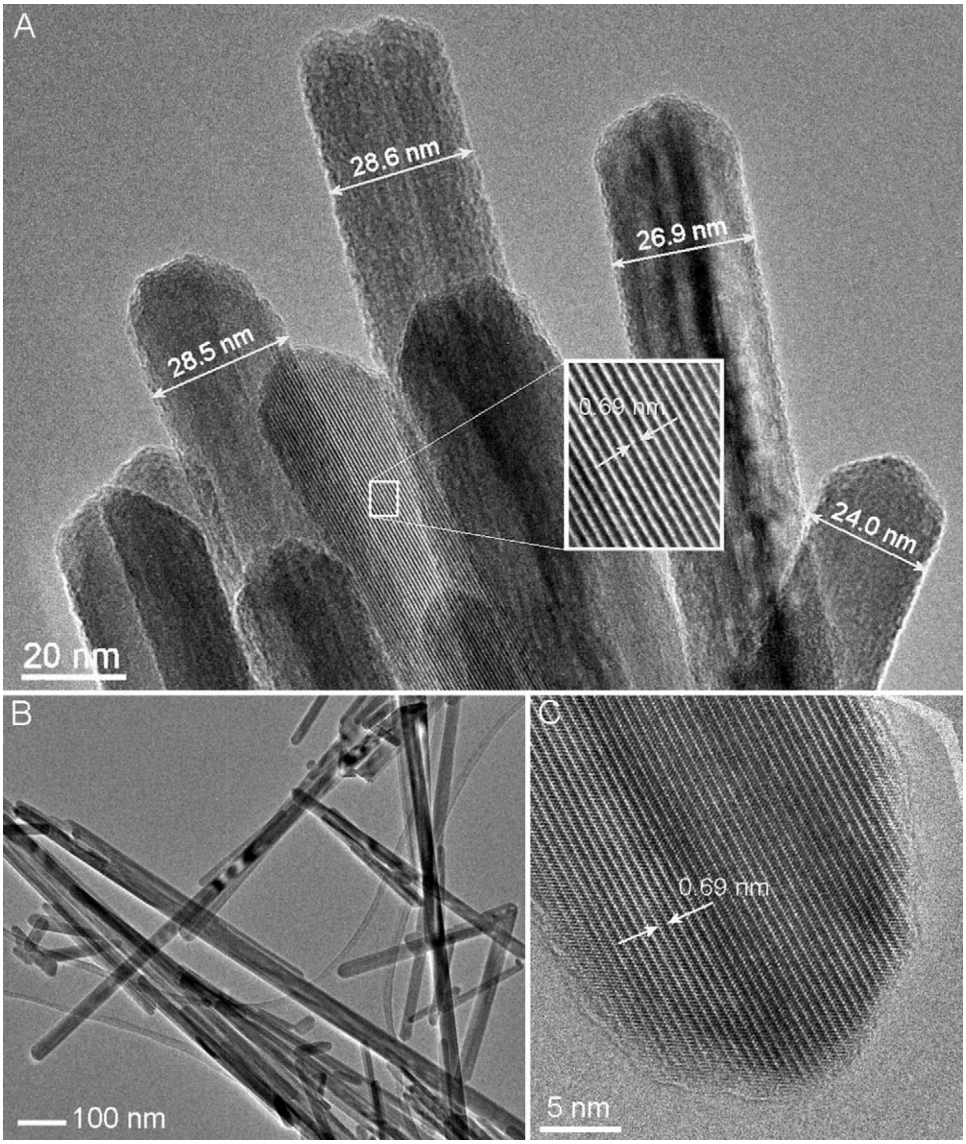

Fig. 4. TEM image of products synthesized: (A) from 4 mmol of $KMnO_4$ (**n-4**). Diameters of the measured nanorods are between 24 and 29 nm. The lattice spacing in the inset is 0.69 nm, (B) from reaction mixture that was kept at 150 °C for 6 h (**t-6**), and (C) for 24 h (**t-24**).

higher [22]. In our case the product prepared at 170 °C is α-MnO_2, like the rest of the products in this reaction batch. Most probably in this case the difference in the particle sizes influences the course of the thermal decomposition. As already mentioned are in the product synthesized at 170 °C found two types of nanoparticles regarding the size (Fig. 2C–E), while the products synthesized at lower temperatures (90, 130 and 150 °C) consist of nanorods. Additional measurements need to be conducted in order to elucidate the process.

Table 2
Mass loss of the products, prepared at different reaction temperatures and different starting concentrations of $KMnO_4$, in separate temperature ranges.

	Δm [25–300 °C]	Δm [300–700 °C]	Δm [700–1100 °C]
Reaction temperature			
T-90	3.60%	8.80%	0.91%
T-150[a]	3.21%	7.26%	5.00%
T-170	2.96%	5.00%	3.71%
$n(KMnO_4)$			
n-1.6[a]	3.21%	7.26%	5.00%
n-4	3.62%	7.63%	6.21%
n-8	7.66%	5.90%	17.33%

[a] Labels **T-150**, **n-1.6** and **t-17** refer to the same sample that was synthesized at 150 °C for 17 h from 1.6 mmol of $KMnO_4$.

The second step at a temperature higher than 500 °C corresponds to the transformation of α-MnO_2 to α-Mn_2O_3, according to the reaction: $2MnO_2(s) \rightarrow Mn_2O_3(s) + 1/2O_2(g)$ [23,24]. The Mn_2O_3 remains stable up to 1100 °C in the case of the product synthesized at 90 °C.

From 700 to 850 °C two decomposition reactions take place simultaneously in the product **T-150**: the reduction of Mn_2O_3 to Mn_3O_4 according to the reaction $3Mn_2O_3(s) \rightarrow 2Mn_3O_4(s) + (1/2)O_2(g)$, and the thermal decomposition of $MnSO_4$ to Mn_3O_4 [25]. Sulfate anions are present in the product due to the preparation procedure and are probably coordinated on the surface of the particles.

In the product **T-170** the reduction of Mn_2O_3 to Mn_3O_4 occurs from 700 to 850 °C. The temperature region of an additional step from 900 to 1100 °C is more typical for the sublimation of K_2SO_4 or its thermal decomposition ($K_2SO_4(s) \rightarrow 2K(g) + SO_2(g) + O_2(g)$) than for the decomposition of $MnSO_4$ [25]. The morphology of this product (short nanorods, short elongated nanoparticles)

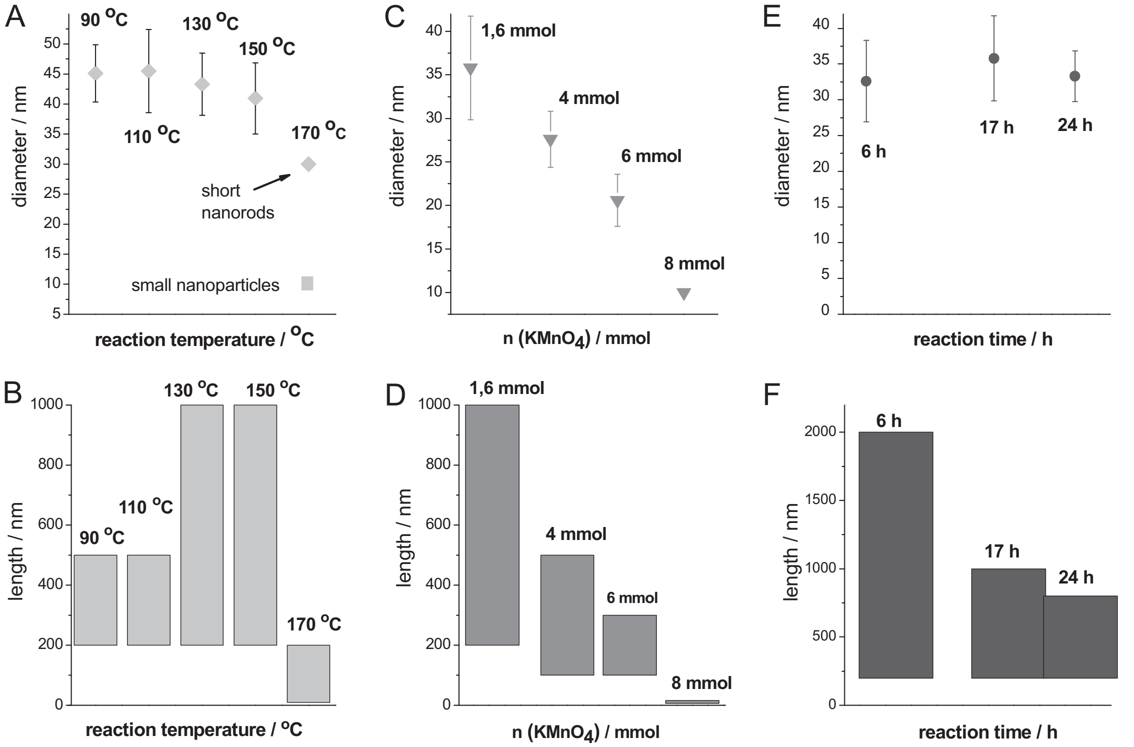

Fig. 5. Diameters and lengths of α-MnO_2 nanorods obtained under different reaction conditions: (A, B) temperature, (C, D) different amounts of mmol of $KMnO_4$, and (E, F) reaction times. Labels **T-150**, **n-1.6** and **t-17** refer to the same sample that was synthesized at 150 °C for 17 h from 1.6 mmol of $KMnO_4$.

probably enables the coordination of sulfate anions on potassium ions, which are located in the channels of the hollandite structure.

In an atmosphere of air the transformation from Mn_2O_3 to Mn_3O_4 occurred at 940 °C [23], whereas in an inert atmosphere this step occurs at a lower temperature, as is evident from Fig. 6C. The weight of the sample starts to increase in the air at temperatures higher than 500 °C, meaning that the oxidation process begins and the reduction to the final product of the thermal decomposition is completed slightly below 1000 °C.

The TG curves of the products obtained from different mmol of $KMnO_4$ (Fig. 6B) reveal the three already described steps. The curves obtained for **n-1.6** and **n-4** (both α-MnO_2 with similar morphology) are nearly identical; only in the third step is a larger mass loss observed for **n-4** (Table 2). The reason is again in the slightly higher content of sulfate ions (Table 1). The TG curve of the product **n-8** exhibits the largest weight losses in the first step (dehydration) and in the last step (oxidation of Mn_2O_3 to Mn_3O_4), when compared to the TG curves of **n-1.6** and **n-4**. As already mentioned, the morphology and crystal structure of this product are totally different from the others in this reaction batch. Again, the mass loss in the third step is connected with the content of sulfate ions, since the content of the sulfate anions was the largest in this sample (Table 1). In addition, the relatively high mass loss in the first step (~9%) is not related to a specific surface area, since this one is rather low (18.5 m^2/g), but also to a higher content of sulfate anions, which are known to possess hydrophilic properties.

The structure of the α-MnO_2 products obtained at different reaction temperatures was further studied with a nitrogen adsorption–desorption experiment (Fig. 7). Interestingly, with an increase in the reaction temperature from 90 to 170 °C the BET surface area is reduced from 45.6 to 33.4 m^2/g. As shown previously, nanorods synthesized at 90 and 130 °C form a secondary structure, and most probably due to this secondary structure, additional adsorption sites are created. Furthermore, isotherms of all three products (figure) exhibit hysteresis loops. For **T-90** the hysteresis

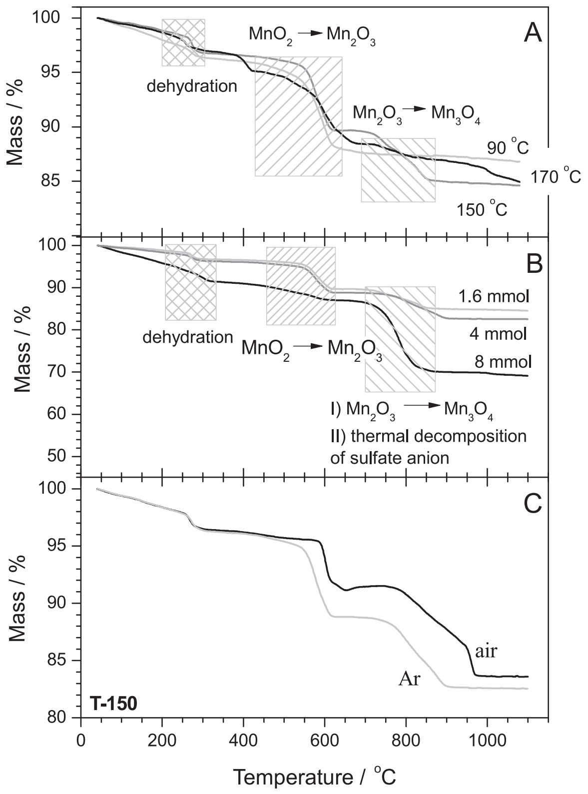

Fig. 6. Dynamic TG curves of the products synthesized: (A) at different reaction temperatures and (B) with different amounts of $KMnO_4$. The influence of the purge gas (Ar or air) on a TG curve is shown in (C) for the product synthesized at 150 °C for 17 h from 1.6 mmol of $KMnO_4$. Labels **T-150** and **n-1.6** (1.6 mmol) refer to the same sample that was synthesized at 150 °C for 17 h from 1.6 mmol of $KMnO_4$.

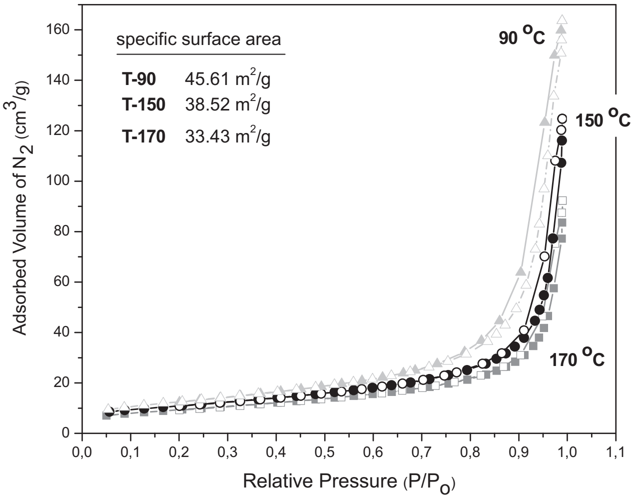

Fig. 7. N_2 adsorption isotherms measured at −196 °C for products synthesized at 90 (**T-90,** triangles), 150 (**T-150**, circles) and 170 °C (**T-170**, squares), with the corresponding specific surface areas.

loop is found in the relative pressure range (P/P_o) of 0.75 to ~0.97, whereas the product synthesized at 170 °C exhibits a similar hysteresis, but in a shorter relative pressure range of 0.90 to ~0.98. According to Ref. [26], the loop at the lower relative pressure range can be ascribed to the presence of a mesoporous structure.

4. Conclusions

In this paper, we have shown that by the selective regulation of reaction parameters at hydrothermal decomposition of $KMnO_4$ the average diameter and length of synthesized α-MnO_2 type of nanorods can be easily tuned. It was clearly demonstrated that the reaction temperature and reaction time have a strong impact on the secondary structure, while the diameter can be easily regulated with the starting amount of $KMnO_4$ in the reaction mixture. The average diameter was reduced by 45% (from 35.9 to 20.6 nm) when the amount of $KMnO_4$ in the reaction mixture was increased by 3.75 times, and at the same time the length span was narrowed from 1000−200 nm to 300−100 nm. The length of the synthesized nanorods can also be easily controlled by the reaction time or by the numbers of mmol of $KMnO_4$ in the reaction mixture.

Acknowledgements

The financial support from the Slovenian Research Agency (project no. J2-9217) is gratefully acknowledged. The authors also acknowledge financial support from the European Union as part of a Framework 6 program under a contract for an Integrated Infrastructure Initiative (reference 026019 ESTEEM) and the COST Action MP0901 “NanoTP”.

References

[1] C. Chouly, D. Pouliquen, I. Lucet, J.J. Jeune, P. Jallet, J. Microencapsul. 13 (1996) 245–255.
[2] T.R. Jensen, M. Malinsky Duval, L.C. Haynes, R.P. Van Duyne, J. Phys. Chem. B. 104 (2000) 10549–10556.
[3] J.M. Bergen, H.A. von Recum, T.T. Goodman, A.P. Massey, S.H. Pun, Macromol. Biosci. 6 (2006) 506–516.
[4] J.E. Post, Proc. Natl. Acad. Sci. U.S.A. 96 (1999) 3447–3454.
[5] A.R. Armstrong, P.G. Bruce, Nature 381 (1996) 499–500.
[6] Y.F. Shen, R.P. Zerger, R.N. DeGuzman, S.L. Suib, L. McCurdy, D.I. Potter, C.L. O’Young, Science 260 (1993) 511–515.
[7] Y. Dong, H. Yang, K. He, S. Song, Z. Zhang, Appl. Catal. B: Environ. (2008), doi:10.1016/j.apcatb.2008.07.007.
[8] C. Xia, W. Ning, G. Lin, Sens. Actuators B 137 (2009) 710–714.
[9] X. Wang, J. Li, J. Chem. Eur. J. 9 (2003) 300–306.
[10] H.J. Kim, J.B. Lee, Y.-M. Kim, M.-H. Jung, Z. Jagličić, P. Umek, J. Dolinšek, Nanoscale Res. Lett. 2 (2007) 81–86.
[11] H. Wang, Z. Lu, D. Qian, Y. Li, W. Zhang, Nanotechnology 18 (2007) 115616.
[12] D. Portehault, S. Cassaignon, E. Baudrin, J.-P. Jolivet, J. Mater. Chem. 19 (2009) 2407.
[13] M.-S. Wu, J.-T. Lee, Y.-Y. Wang, C.-C. Wan, J. Phys. Chem. B 108 (2004) 16331.
[14] V.G. Kuar, K.B. Kim, Ultrason. Sonochem. 13 (2006) 549.
[15] H. -en Wang, D. Qian, Z. Lu, Y. Li, R. Cheng, W. Zhang, J. Cryst. Growth (2007), doi:10.1016/jcrysgro.2007.01.034.
[16] P. Umek, A. Gloter, M. Pregelj, R. Dominko, M. Jagodič, Z. Jagličić, A. Zimina, M. Brzhezinskaya, A. Potočnik, C. Filipič, A. Levstik, D. Arčon, J. Phys. Chem. C 113 (2009) 14798.
[17] J. Luo, H.T. Zhu, H.M. Fan, J.K. Linag, H.L. Shi, G.H. Rao, B. Li, Z. Du, J. Phys. Chem. C 112 (2008) 12594.
[18] T. Sugimoto (Ed.), Fine Particles, Parts I and II, Marcel Dekker Inc. A series of articles published in MRS Bull. 14 (1989) and 15 (1990).
[19] C.E. Housecroft, A.G. Sharpe, Inorganic Chemistry, 3rd ed., Pearson Education Limited, England, 2008.
[20] D.A. Skoog, D.M. West, F.J. Holler, Fundamentals of Analytical Chemistry, 6th ed., Sounders College Publishing, 1992.
[21] L. Li, Y. Pan, L. Chen, G. Li, J. Solid State Chem. 180 (2007) 2896.
[22] R. Giovanoli, Thermochim. Acta 234 (1994) 303.
[23] Z.-Y. Yuan, Z. Zhang, G. Du, T.-Z. Ren, B.-L. Su, Chem. Phys. Lett. 378 (2003) 349.
[24] R. Ma, Y. Bando, L. Zhang, T. Sasaki, Adv. Mater. 16 (2004) 918.
[25] P. Bukovec, N. Bukovec, Ž.D. Živkovič, (Eds.), Thermal Analysis (Thermal Decomposition of Sulfates), Collection of Papers, Bor, Yugoslavia, 1984.
[26] M. Xu, L. Kong, W. Zhou, H. Li, J. Phys. Chem. C 111 (2007) 19147.